Journal of Alloys and Compounds 900 (2022) 163430

Contents lists available at ScienceDirect

Journal of Alloys and Compounds

journal homepage: www.elsevier.com/locate/jalcom

High-heat flux Cu-0.8Y alloys investigated by positron annihilation spectroscopy

R. Domínguez-Reyes[a,*], M.A. Monge[a], B. Galiana[a], Y. Ortega[b], A. Muñoz[a], G. Carro-Sevillano[c]

[a] Departamento de Física. Universidad Carlos III de Madrid, 28911 Leganés, Madrid, Spain
[b] Departamento de Física de Materiales. Facultad de Ciencias Físicas. Universidad Complutense de Madrid, 28040 Madrid, Spain
[c] Centro Nacional de Investigaciones Metalúrgicas (CENIM-CSIC), Departamento de Metalurgia Física, Avd. Gregorio del Amo 8, 28040 Madrid, Spain

ARTICLE INFO

Article history:
Received 20 September 2021
Received in revised form 24 November 2021
Accepted 22 December 2021
Available online 24 December 2021

Keywords:
Copper alloys
Oxide dispersion strengthened
Positron annihilation
High-heat flux materials
Equal channel angular pressing
Reinforced materials

ABSTRACT

This work studies the thermal stability of the microstructure and the evolution of the defects of two high-heat flux Cu-0.8 wt%Y alloys fabricated following two alternative powder metallurgy routes. One batch was produced by direct hot isostatic pressing (HIP) consolidation of Cu-0.8 wt%Y pre-alloyed atomized powders while an additional ball milling processing step was introduced before HIP sintering for the second alloy. The stability and recovery characteristics of the vacancy type defects in these alloys in the as-produced state and after processing by severe equal channel angular pressing to achieve a refine microstructure have been investigated by positron lifetime and coincidence Doppler broadening measurements in samples subjected to isochronal annealing from room temperature to 900 °C. Microhardness measurements and electron transmission microscopy analysis have also been performed to support the results obtained from the positron annihilation spectroscopy analysis techniques. The recovery curves of the positron lifetime and S-W plots show a recovery stage in agreement with the recovery stage V for Cu. However, a full recovery is not accomplished, and a stage that reverts the previous recovery takes place after annealing above ~600 °C, that leads to the formation of very stable defects at temperatures up to 900 °C, identified as vacancy aggregates and nanocavities. The characteristic shape of the coincidence Doppler broadening indicates that the dispersed Y-O particles in the Cu matrix appear to be responsible for stabilizing the vacancy aggregates and nanocavities for temperatures above 600–700 °C.

1. Introduction

Dispersion strengthened (DS) and precipitation hardened (PH) Cu alloys are primary candidate materials for heat sink applications in the plasma facing components (PFCs) of a near-term DEMO fusion reactor due to their high thermal conductivity, enhanced mechanical strength and irradiation resistance [1–4]. They have to be thermally stable and radiation, creep and fatigue resistant at elevated temperatures, under the severe working conditions required for DEMO; such as heavy thermal loads near the upper working temperature of the materials, repeated stepwise changes in temperature and heavy high-energy particle irradiation [5]. PH CuCrZr and DS Cu-Al_2O_3 (GlidCop) are presently the baseline high-heat flux (HHF) materials in the water-cooled PFCs designs for the near-term DEMO as there exists an important database that has allowed to predict their performances under the ITER operation conditions [6,7]. However, PH CuCrZr at temperatures above 400 °C is susceptible of thermal softening due to over ageing and suffers irradiation embrittlement at temperatures below 200 °C [1,2,7,8]. Moreover, DS Cu-Al_2O_3 and PH CuCrZr exhibit significant thermal creep at temperatures above ~ 350 °C for applied stresses above 60 MPa [8,9]. These HHF materials having critical limits in their working temperatures, i.e. 200 – 350 °C, would lower the overall efficiency of the reactor [10]. The formation of stable stacking faults, voids or bubbles in Cu-based materials is very dependent on multiple factors: alloying elements, presence of reinforcing particles, the irradiation temperature or the presence of thermal cycling, between others [3,4,11–14]. For example, stacking fault tetrahedra (STF) are commonly observed in pure copper, while the presence of dispersed particles, the irradiation at high temperatures or the thermal cycling tend to suppress its formation [3,13].

To develop new high-strength and heat-resistant Cu alloys with a more favorable working temperature window, DS Cu-0.8 wt%Y alloys have been produced by different powder metallurgy routes and their microstructural, thermal and mechanical characteristics have been

* Corresponding author.
E-mail address: rdomingu@fis.uc3m.es (R. Domínguez-Reyes).

https://doi.org/10.1016/j.jallcom.2021.163430
0925-8388/

investigated [15–17]. The results have demonstrated the feasibility of strengthening Cu by dispersion of Y-rich particles maintaining a high thermal conductivity. These alloys as heat sink materials to be joined to PFCs could be exposed at temperatures as high as ~900 °C during the joining operation changing their microstructure and degrading the mechanical properties.

However, materials produced through a powder metallurgical route usually have a higher number density of defects than the observed for similar materials produced by traditional techniques such as casting. The presence of a significant concentration of light impurities, point defects, interstitial-vacancy complexes or voids are commonly observed and have a strong effect in the properties of the material; for example, the presence of vacancy aggregates and voids induce material hardening, loss of ductility and embrittlement [18,19].

The objective of the present study is to investigate the presence and stability of the open volume defects in the studied DS Cu-Y alloys, their stability with the temperature and the interaction of these defects with the dispersoids, impurities and grain boundaries. Isochronal annealing and positron annihilation experiments have been accomplished in the DS-0.8Y alloy processed under different conditions, supported by transmission electron microscopy (TEM) observations in selected samples, to investigate the initial observed recovery up to intermediate temperatures and subsequent formation of voids on increasing temperature.

2. Experimental procedure

DS Cu-Y alloys were produced using powder with a nominal composition Cu-0.8 wt%Y and particle size < 120 μm produced by vacuum induction melting and subsequent atomization in high purity Ar gas. The purity of the initial raw Cu and Y materials was 99.9% and 99.8%, respectively. The atomized powder was consolidated by HIP and the obtained alloy is labeled as CuY. To homogenize and refine the initial microstructure of the atomized powder, a second ingot was produced by milling the initial powder in a high energy planetary ball mill during 40 h at 100 rpm under an Ar atmosphere. In this case, the alloy resulting after HIP consolidation was labeled as CuYM. The milling media were Cr-steel balls with a ball/powder ratio of 5:1. For both materials, the HIP consolidation was performed for 2 h at 1123 K and 179 MPa. Previously, the powder was encapsulated into a steel can that was tightly sealed after degassing at 573 K for 24 h in vacuum. Billets of CuY and CuYM with dimensions of 10 × 10 × 70 were deformed by equal channel angular pressing (ECAP) at 623 K via B_C route, i.e. the billet is rotated + 90° around its longitudinal axis between successive passes. The CuY billet was submitted to 8 passes and the CuYM one to 4 passes, and were denoted as CuYE and CuYME, respectively. Density measurements were carried out in a He ultrapycnometer. The oxygen content was determined in an infrared absorption spectrometer. The microstructure of the alloys was analyzed by ultra-high-resolution scanning electron using a TENEO (FEI) microscope. The processing details and the microstructural, mechanical and thermal properties of these alloys have been reported elsewhere [15–17].

The Positron Annihilation Spectroscopy (PAS) experiments were performed on samples of four materials after being isochronal annealed for 20 min up to 900 °C in a vacuum of < 10^{-5} mbar. Complementary experiments were also performed on samples of pure Cu in different conditions. Positron lifetime measurements were carried out in a fast-fast coincidence spectrometer with a time resolution of 230 ps (FWHM) using a ^{22}Na source sealed in kapton sandwiched between a pair of identical samples. Positron lifetime spectra with a total count number > 10^6 were recorded and analyzed using the PATFIT-88 [20]. The instrumental time resolution and contribution of the positron source to the lifetime spectra were determined from measurements on reference samples of annealed pure Fe and Si single crystals. The source contribution was assessed in a component of 382 ps with an intensity of 13.6% and another very weak of 1.2 ns and 0.2%.

The coincidence Doppler broadening (CDB) measurements were done using two HP Ge detectors in timing coincidence, placed face to face with the samples at the half-way point between the detectors. The resulting CDB spectrum was the cumulative spectrum of 24 CDB spectra without evidence of electronic shift, each of them with a count number > 10^6 in a 512 × 512 coincidence matrix. The cumulative spectra had 1 × 10^7 counts in the strip centered on the matrix diagonal for the energy range $2m_oc^2$-1.6 keV < $E_1 + E_2$ < $2m_oc^2$ + 1.6 keV; E_1 and E_2 stand for the energies of the pair of annihilating photons, m_o the electron rest mass and c the light speed. The spectra were binned from 40 to 512 bins with a bin width of 2.5 × 10^{-3} m_oc to decrease the statistical fluctuations of the data in the high momentum region. The spectra were normalized, and the intensity at a given photon momentum divided by the corresponding counts in the CDB spectrum of a reference sample of pure Cu to highlight the differences between the spectra. 99.999% pure Cu annealed at 900 °C and Y_2O_3 single crystals were used as reference samples. To determine the experimental error bars of CDB curves, it has been considered the mean deviation between independently obtained CDB curves for the same samples, since it is representative of the consistency of the measurements. The fraction of positrons annihilated with low- and high-momentum electrons was also estimated using the S and W line shape parameters. The S parameter was calculated as the ratio of the count number in the energy window of 1.946 keV centered at 511 keV ($p_L \approx 0 - 7(10^{-3}m_0c)$) to the count total in the annihilation peak. The W parameter was calculated as the fraction of counts in the energy intervals 515.66 – 519.72 keV and 502.67–506.74 keV ($p_L \approx 16 - 32(10^{-3}m_0c)$).

Samples at selected annealing temperatures have been also characterized by means of TEM to observe the open volume defects. For that purpose, the TEM images have been achieved focused and out of focus. Samples were examined in a Philips Tecnai F20 operated at 200 kV. Cross-sectional samples were prepared for electron transparency using a focused ion beam (FIB), protecting the sample surface through pre-deposition of a Pt layer, and milling with Ga^+ ions close to normal incidence.

3. Results

3.1. General description of the microstructure

The four studied materials present a similar fully dense microstructure consisting of a copper matrix of equiaxed grains reinforced with a dispersion micrometric and sub-micrometric particles of Y rich oxides located at the grain boundaries and inside the grains. The main differences between them are:

i. The mean grain size of CuY and CuYM after HIP consolidation is micrometric, (3.1 ± 1.6) μm and (2.4 ± 1.6) μm respectively, while after ECAP processing a reduction of the mean grain size of (0.5 ± 0.2) μm for CuYE and CuYME is achieved.
ii. As a result of the milling process prior to HIP consolidation, the CuYM has a more homogeneous and a finer distribution of the reinforcing yttrium-enriched particles than CuY. The ECAP processing produced two materials with similar microstructure characterized by a refinement of the grains and reinforcing particles. The observed Y-O particles are very stable with the temperature and no significant changes on their size or composition have been observed in all the range of the annealing temperatures.
iii. The presence of a significant number of twins in the CuYM is observed. However, the ECAP processing drastically reduced the density of twins.

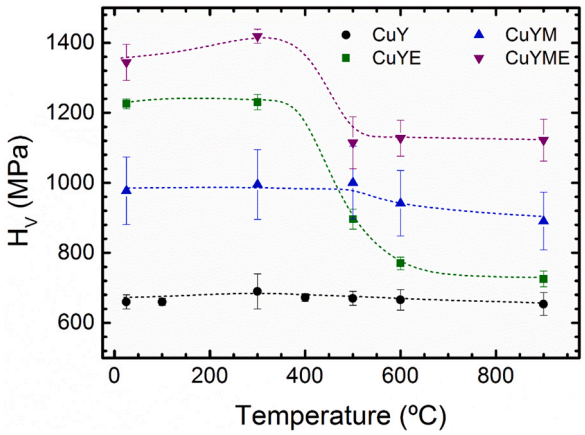

Fig. 1. Microhardness measurements obtained at RT as a function of the isochronal annealing temperature.

iv. Cavities or microvoids were not observed in any of the materials after their production process.
v. ECAP B_C processing route is the best for achieving grain refinement [21,22]. The specific geometry of the ECAP channel used in this work introduces a homogeneous shear strain per pass of 2.03 that results in an equivalent strain of $\varepsilon = 1.17$ per pass [21,22].
vi. CuY and CuYM do not exhibit significant changes in their hardness after the annealing treatments; however, CuYE and CuYME exhibit an important reduction of the hardness for temperatures higher than 300 °C and decrease to similar values to CuY and CuYM for temperatures ≥ 600 °C, respectively (see Fig. 1).

A detailed description of the microstructure and mechanical properties of these materials after consolidation by HIP and different thermo-mechanical treatments, including ECAP, has been already published [15–17]. As reference, Fig. 2 presents the main characteristics of the CuYM microstructure. A bright-field TEM micrograph showing a general view of the as-HIP material, consisting of equiaxed grains, is depicted in Fig. 2(a). Fig. 2(b) and the subfigures (b_1), (b_2) and (b_3) correspond to a STEM image and the corresponding EDS elemental maps of the Y-O reinforcing particles. The presence of dislocation tangles is observed in some grains, as it is shown in the subfigure 1(a). The elemental composition of the different phases present in the CuYM was established by numerous EDX measurements. As can be observed in the two examples shown in Fig. 2(c), the reinforcing particles are composed of Y and O while the matrix is pure Cu.

3.2. Positron lifetime measurements

The lifetime spectra are characterized by a single lifetime value, τ, the evolution of which with annealing temperature is summarized in Fig. 3. Neither of the measured lifetime spectra could be consistently fitted to a sum of two or more lifetime components even if a long-lived lifetime value is constrained to any of the expected positron lifetime for defects in Cu (see Table 1). The unmilled CuY in the as-HIP condition exhibits a pronounced recovery stage of the measured mean positron lifetime starting at ≈ 200 °C and finishing at ≅ 600 °C, with a reduction of the measured positron lifetime from a value of 172 ps to a minimum of 133 ps (see Fig. 3(a)). This recovery is followed by a stage that reverts it that finishes after annealing at T ≥ 700 °C, reaching a value of 157 ps that remains constant up to the maximum annealing temperature of 900 °C. As shown in Fig. 3(a), the mean lifetime values obtained for the isochronal annealing process of the CuYM exhibits a similar behavior with the curve, shifted to higher values. The initial τ value before recovering at 200 °C is roughly 180 ps, decreasing to a minimum of 168 ps at 600 °C to increase to a steady value of ≈ 178 ps for temperatures higher than 700 °C.

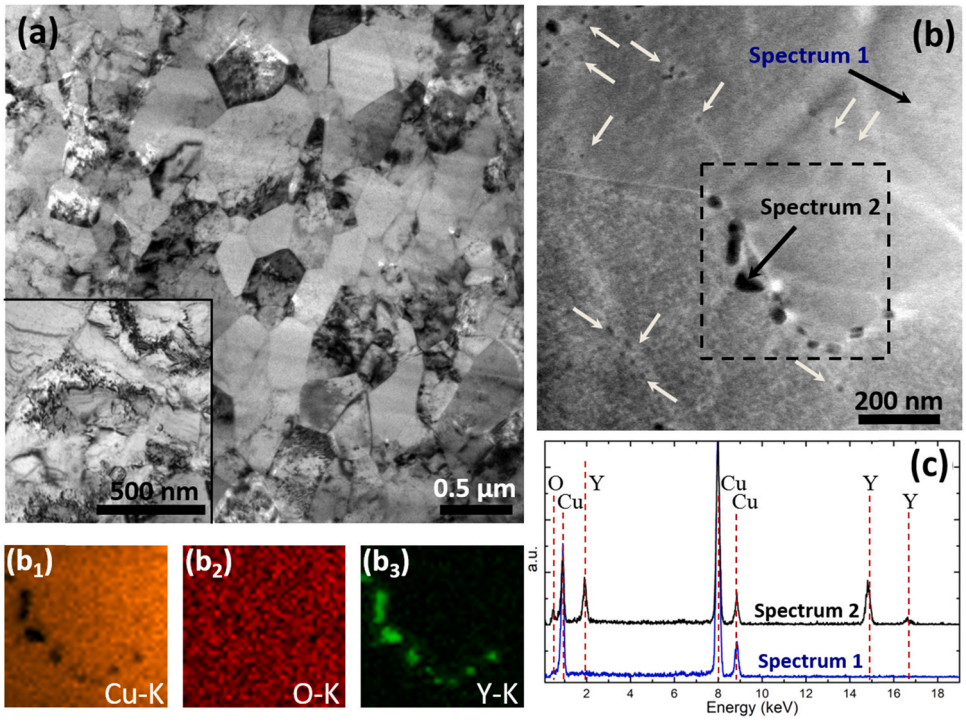

Fig. 2. Main characteristics of the microstructure of the CuYM. (a) BF-TEM image showing a general view of the equiaxed grain microstructure of CuYM. The sub-figure (a) reveals the presence of dislocations tangles. (b) STEM image and EDS elemental maps of the marked region showing the Y-O reinforcing particles: (b1) HAADF-STEM image, (b2) O-K and (b3) Y-K. (c) EDX measurements at the points indicated by arrows in (b) revealed that the reinforcing particles are composed of Y and O, and the matrix is pure Cu. White arrow points to numerous nanometric Y-rich particles present in the Cu matrix.

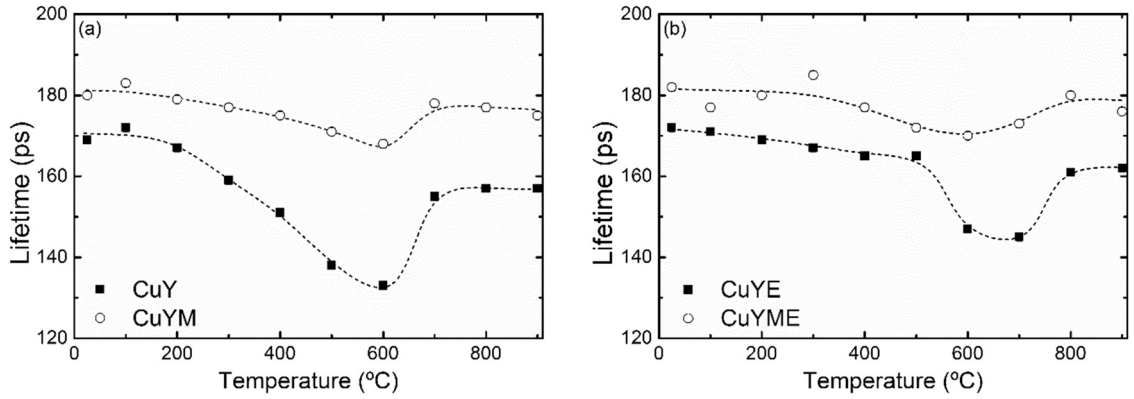

Fig. 3. Positron annihilation spectroscopy measured lifetimes as a function of annealing temperature for: (a) CuY and CuYM after HIP consolidation, (b) CuYE and CuYME after ECAP processing.

Table 1
Experimental, τ_{Exp}, and theoretical, τ_{Th}, values of the positron in pure Cu and Cu defects. The presented values correspond to results that have been confirmed by several works. Some theoretical predictions derived from different framework calculations are also presented. References to some representative literature works are included. The τ_{Th} values range from divancancies up to aggregates of 40 vacancies (*).

	τ_{Exp} (ps)	Reference	τ_{Th} (ps)	Reference
Pure Cu	106 – 122	[32–34]	108 – 113	[34,35]
Dislocation	–	–	122	[34]
monovacancy	158 – 166	[32,34]	166	[34,35]
Dislocation + vacancy	166 – 176	[36]	179	[34,37]
Divacancy	–	–	180 – 190	[34,36,38]
Vacancy aggregates/ voids	340 – 500	[38,39]	180 – 400(*)	[34]

For both materials, the evolution of the values with the annealing temperature after ECAP processing is shown in Fig. 3(b) and presents a similar overall shape to the observed for the unprocessed materials CuY and CuYM with a lower variation range of τ. The CuYE initiates the recovery at higher temperature than the CuY, at ≈ 350 °C, and also finishes at a higher temperature, ≈ 700 °C. After a short process where the recovery is reverted, the value of τ increases to a constant value of ≈ 162 ps for temperatures ≥ 800 °C, similar to the observed one for CuY at high temperatures.

The samples of the CuYM material in the as-HIP or ECAP processed states have very similar values in all the temperature range of the isochronal annealing treatments (see Fig. 3). The only significant differences are higher values of τ for all the annealing temperatures and a lower slope at the state after reverting the recovery on increasing temperature.

3.3. CDB measurements

The ratio CDB curves of the materials and their evolution with isochronal annealing are shown in Fig. 4 and Fig. 5 for selected annealing temperatures.

As reference, the ratio CBD curves of a high purity samples of Y_2O_3 (using 99.99% purity nanopowder compacted before and after vacuum sintering at 1400 °C) and a well annealed elemental Y (99.98% purity at 1000 °C) are also depicted in Fig. 6. Both reference CDB curves present the higher values at low momentum, $p_L \approx 0$ of all measured CDB spectra and a characteristic structure at the intermediate momentum region, $p_L \approx 5 - 30(10^{-3}m_0c)$, showing the Y_2O_3 distinctive peaks that are clear revealed in CDB_{Y2O3}/CDB_Y normalized spectrum (see Fig. 6). Its characteristic shape provides the characteristic signature of positron annihilation with Y in copper or oxygen anions in Y_2O_3. The trapping and subsequent annihilation of positrons with this Y-O oxides or Y aggregates is expected due to the very high positron affinity of Y and oxygen anions in the Y-O oxides [23,24], which are the highest compared to Cu or any other elements present in the studied materials including light impurities like C, or Cr and Fe from the grinding media [25]. The CDB_{Y2O3}/CDB_Y ratio curve is especially interesting because yttria has been poorly studied with positrons techniques and presents a complex crystalline structure, having a less ionic character than other similar oxides, which may result in a CDB spectrum with a significantly different shape that the reported for other widely studied oxides, such as Al_2O_3, MgO or SiO_2 [26–29] and references therein. It highlights the characteristics of the momentum distribution of the oxygen anions core electrons of the Y oxide, that are significantly different to the found for other similar oxides.

As it is observed in Fig. 4(a) for CuY, the low momentum peak at $p_L \approx 0$ decreases on increasing temperature up to the annealing temperature of 600 °C where the minimum value is reached, with the corresponding increase of the CDB curves at the intermediate momentum region. After annealing at 700 °C, the low momentum peak increases, with a corresponding decrease in the intermediate momentum region, remaining the CDB curves similar for higher annealing temperatures (Fig. 4(b)). A similar but less pronounced behavior is observed for CuYM in Fig. 5(a) and (b). Finally, the CDB curves for the ECAP processed materials exhibit the same overall shape and annealing behavior than the one corresponding to their respective materials in the as-HIP condition (see Fig. 4(c) and (d), and Fig. 5(c) and (d) for the CuYE and CuYME, respectively).

Figs. 7 and 8 show the correlation plots of the *W* values versus *S* calculated for the different annealing temperatures for all the materials. Relative values for *W* and *S* parameters were used (instead of the directly calculated values) for a better comparison. Well annealed 99.999% pure Cu was used as reference, so its *W* and *S* parameter values were used to normalize all the studied sample parameters.

The value obtained from heavily deformed cold-work 99.999% pure Cu is shown as reference. These plots are useful for revealing the presence of different positron traps or changes in the chemical surrounding of the positron annihilation sites during isochronal annealing.

In the case of positron annihilation taking place in two positron states, i.e. in a free state and in a trapped state in a single type of defect, or otherwise in two trapped state in two different types of defect, it is known that the measured line shape parameters *S* and *W* are given by

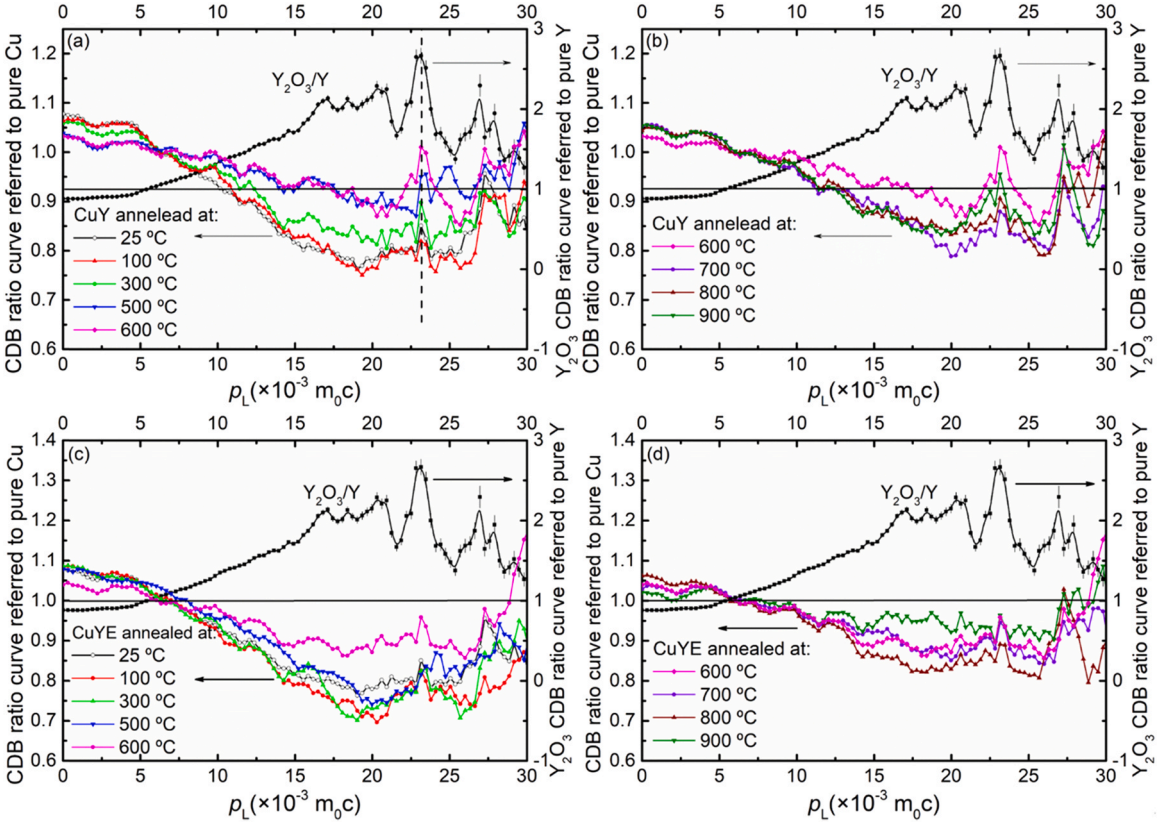

Fig. 4. CDB ratio curves measured at selected temperatures of the isochronal annealing treatment (a) for CuY from 25 °C to 600 °C and (b) 600 °C to 900 °C; (c) for CuYE from 25 °C to 600 °C and (d) 600 °C to 900 °C. Studied Cu samples CDB ratio curves are normalized to a well annealed high purity Cu sample. For comparison, the CDB normalized ratio curve of a highly purity Y_2O_3 sample is shown. Error bars have been included only for the Y_2O_3 curve for clarity purposes. Equivalent error bars should be considered for the rest of the curves.

$$S = (1 - f_2)S_1 + f_2 S_2$$
$$W = (1 - f_2)W_1 + f_2 W_2 \quad (2)$$

where f_2 is the fraction of annihilations in the state 2, $_{Si}$ stands for the line shape parameters representative of the annihilations with the low momentum valence electrons for each state, and W_i the corresponding with the high momentum electrons. From Eq. 2 the following correlation is found

$$W = -RS + (W_2 + RS_2) \quad (3)$$

where R is a constant defect-specific parameter independent of the number density of positron traps given by [30].

$$R = \frac{W_1 - W_2}{S_2 - S_1} = \frac{W - W_2}{S_2 - S} \quad (4)$$

Then, if the *W-S* plot exhibits a linear dependence, either a single type of defect acts as positron traps or there exists positron trapping saturation in two effective defects, or positron traps with similar positron affinity, through the recovery and isochronal annealing. In most of the annealing conditions, positron trapping saturation at open volume defects appears to be the case for either alloy in the as-HIP condition or after being ECAP deformed. Nevertheless, the apparent linear dependence of the *W-S* plots may be misleading and requires a careful analysis of the variations of consecutive points in the *W-S* plots with their isochronal annealing temperature, as will be discussed below.

3.4. TEM measurements

The presence of nanovoids was studied by bright-field TEM using a through-focal technique, being the under/over focus distance of 0.5 µm. The observations were carried out on samples CuY in the as-HIP state, and in CuYE samples after the annealing treatment at 600 °C and 900 °C. The presence of nanocavities in the CuY and CuYE was not observed after HIP consolidation. Fig. 11 gathers the set of measurements to different focal lengths.

In the sample annealed at 600 °C, the observed nanovoids are mainly located on grain boundaries; while in the annealed sample at 900 °C they appear both randomly dispersed in the matrix and on the grain boundaries.

4. Discussion

The interpretation of the positron lifetime and CDB experiments in the studied materials is not straightforward due to the impossibility to resolve the positron lifetime spectra into several components irrespective of the temperature of the annealing treatment or the initial microstructure of the materials (two-component fit provided non-reliable results). This suggests the presence of a mixed set of annihilation sites with similar characteristic positron lifetime that compete as positron traps. The trapping saturation at a unique type of defect is discarded due to the observed changes of the measured positron lifetime and the S-W plots with the temperature [31] (see Figs. 3 and 7), therefore the single lifetime component will also be considered as an average lifetime, since it includes the annihilation in several types of positron traps and several components were not separated. The variation observed in the S-W plots discards positron trapping saturation in a single positron traps because the value of both parameters is an intrinsic characteristic of the type of defect. The single lifetime τ of CuY and CuYM in the as-HIP condition remains almost unchanged to τ ~ (170 ± 3) and (180 ± 4) ps, respectively, from room temperature up to ~200 °C, indicating the

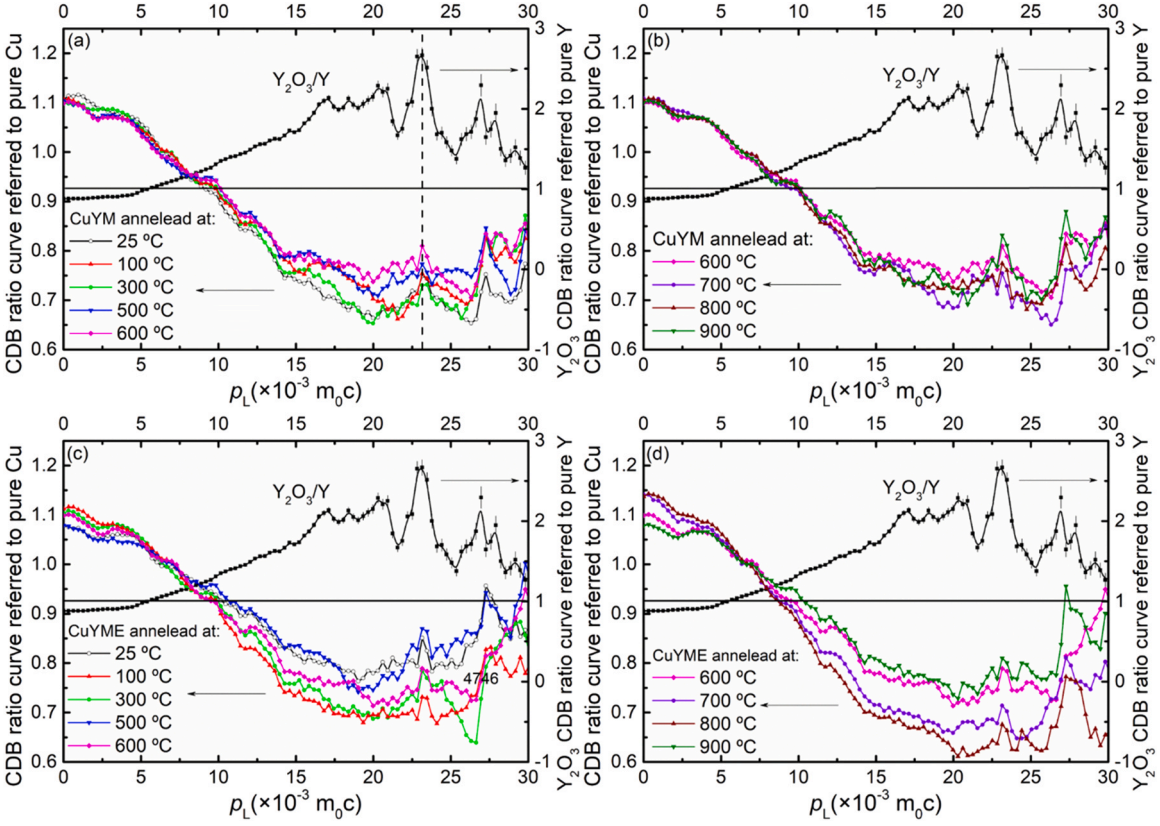

Fig. 5. CDB ratio curves measured at selected temperatures of the isochronal annealing treatment (a) for CuYM from 25 °C to 600 °C and (b) 600 °C to 900 °C; (c) for CuYME from 25 °C to 600 °C and (d) 600 °C to 900 °C. Studied Cu samples CDB ratio curves are normalized to a well annealed high purity Cu sample. For comparison, the CDB normalized ratio curve of a highly purity Y_2O_3 sample is shown. Error bars have been included only for the Y_2O_3 curve for clarity purposes. Equivalent error bars should be considered for the rest of the curves.

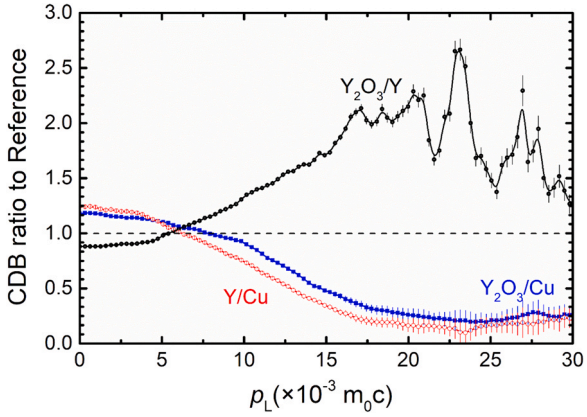

Fig. 6. Ratio CDB curves of Y2O3 and pure Y, divided by the reference annealed pure Cu. The ratio CDB curve of Y2O3 to pure Y is also depicted and shows the predominant characteristics of the CDB spectra associated with core electrons of the oxygen anions of the Y oxide.

presence of stable defects in that range of temperatures due to its high value compared with the expected for defect-free Cu. Table 1 summarizes the characteristic values of the positron lifetime for pure copper and its defects that have been confirmed by several works in the literature (see references in the table caption). Values of τ of 170–180 ps are representative either of competitive positron trapping and annihilation in different types of defects such as vacancy aggregates, nanovoids and vacancy complexes attached to dislocation, or at the Y-O particles and grain boundaries.

Fig. 9 shows the temperature dependence of the S value for CuY in comparison with the values obtained for well annealed high-purity Cu (defect-free), and heavily cold-deformed high-purity Cu (thickness reduction of 50%). The S values in the temperature range of 25–200 °C are similar to cold-deformed pure Copper, where it has been well established in the literature that vacancy-like defects, vacancy agglomerates and vacancy-dislocations complexes are responsible of the positron annihilation (see [40,41] and references therein). This result agrees with the observed for the positron lifetime that exhibits the same dependence as S parameter over the whole temperature range (both compared in Fig. 9).

The decrease of the positron lifetime to its minimum value of 133 ps is caused by a recovery stage in CuY that initiates at temperatures around ~300 °C and finishes at 600 °C (see Fig. 3). The onset and end temperature of the recovery process is shifted to higher values for CuYE, being the minimum lifetime of 145 ps reached at a temperature 50 °C higher than the observed for CuY. Fig. 9 also shows the recovery of the CuY, with the expected decrease of the S values on increasing temperature up to values near of the defect-free Cu, which can be attributed to the dissociation and annealing of vacancy aggregates in the Cu matrix. This recovery stage, that can be clearly followed in the plot of the (S, W) values that follows the same linear trend with temperature that the recovery of cold deformed high purity Cu to a thickness reduction of 50% (see Fig. 7(a) and (b)). These results seem to indicate that the annealing vacancy-related defects in these materials behave similarly to the well-studied recovery of irradiated or heavily deformed Cu. The annealing behavior of point defects and dislocations in pure copper and single-phase Cu alloys progresses gradually through five recovery stages [38,42–45]. The initial stages start at low temperature being stages III and IV corresponding to the recombination of migrating vacancies with interstitials, and the formation of new vacancies released by the dissociation of clusters. Stage V ends with

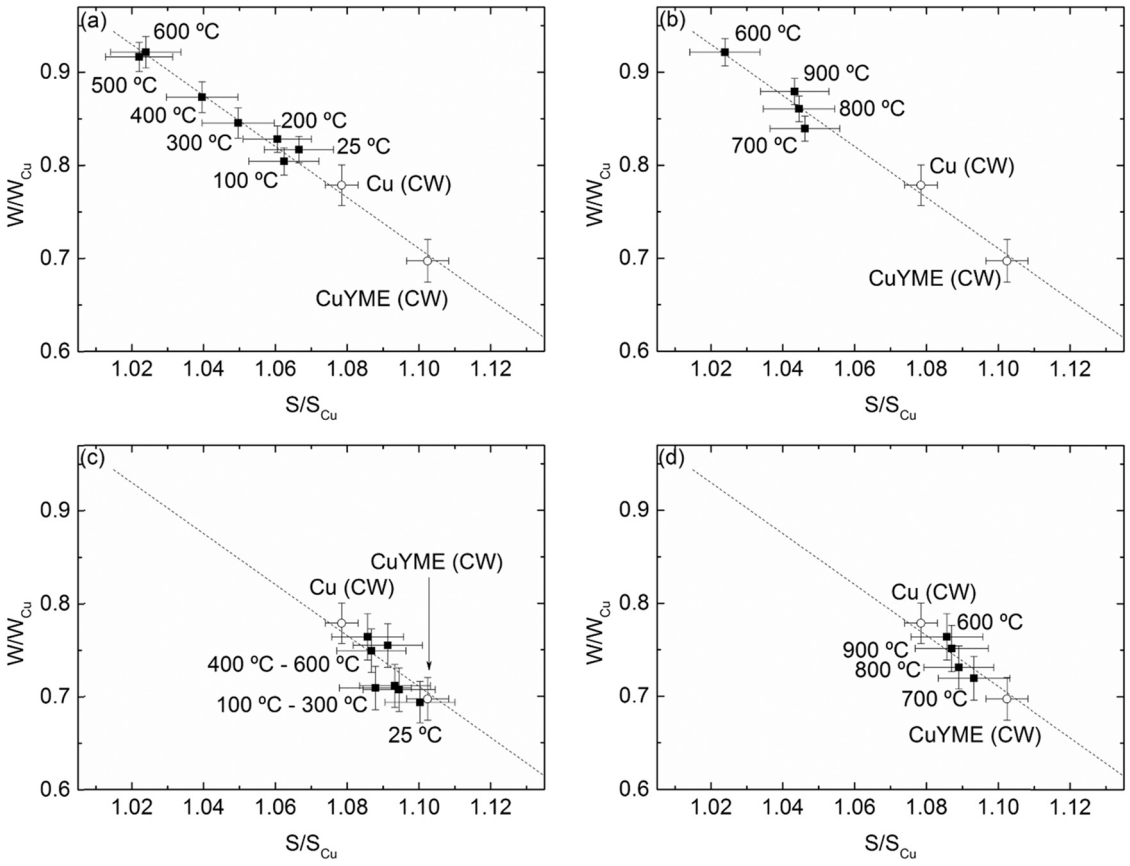

Fig. 7. Relative S-W plots for CuY, (a)-(b), and CuYM, (c)-(d), where the annealing temperatures are shown in the ranges 25 °C to 600 °C and 600 °C to 900 °C. All values are relative to pure annealed Cu. For reference, the values for high purity deformed Cu (cold-worked 50% thickness reduction) are shown, also, the relative S-W pair for CuYME cold-worked.

the full recovery of the microstructure at ≈ 450 °C when Cu has been subjected to extreme plastic deformation [46–49]. Even though recovery and recrystallization are competitive phenomena, at higher temperatures the changes in the microstructure are caused by grain growth. In the studied Cu reinforced materials, the presence of light impurities and precipitates, such as C or O, and Y-O particles can increase the temperature of the recovery processes [50].

However, CuY and CuYM have been submitted to a high sintering temperature of 850 °C, and therefore recovery should have been completed in the materials prior to the isochronal annealing treatments where the measurements have been performed. The presence of these vacancy-type defects in the as-HIP materials is due to two main reasons. CuY and CuYM were quenched from the sintering temperature to 350 °C in a short time of ≈ 15 min (cooling from that temperature to 50 °C inside the furnace took a time of ≈ 60 min), retaining vacancy-like defects produced from the high number of thermal activated vacancies at the sintering temperature. Also, the mismatch between the thermal expansion coefficients of the steel container and the reinforced Cu, 14.4×10^{-6} K^{-1} for the steel, and $(18.5 \pm 0.1) \times 10^{-6}$ K^{-1} and $(17.7 \pm 0.2) \times 10^{-6}$ K^{-1} for the CuY and CuYM respectively, can produce strain in the sintered materials at cooling [51].

CuYE and CuYME follow the same behavior, with a larger positron lifetime and varying within a narrower range (See Fig. 3(b)).

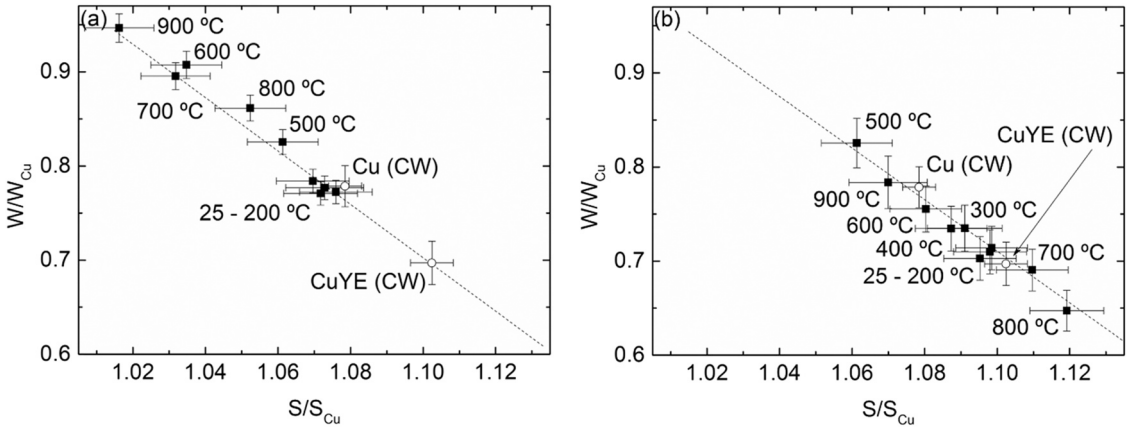

Fig. 8. Relative S-W plots for (a) CuYE and (b) CuYME where the annealing temperatures are shown. All values are relative to pure annealed Cu. For reference, the values for high purity deformed Cu (cold-worked 50% thickness reduction) are shown, also, the relative S-W pair for CuYME cold-worked.

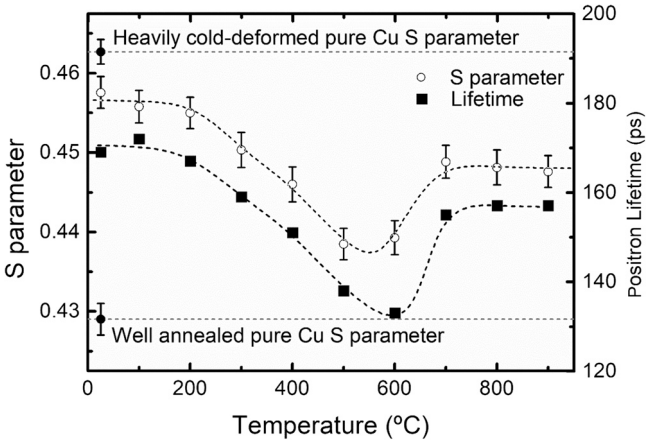

Fig. 9. S parameter as a function of the annealing temperature for CuY compared to measured positron lifetime. The values for high purity Cu defect-free after annealing and heavily deformed (cold-worked 50% thickness reduction), are shown for reference.

Severe plastic deformation processing, such as ECAP, produces a remarkable transformation in the microstructure of these alloys, giving rise to a high density of dislocations that dynamically reorganize to form low and high angle boundaries and vacancy-like defects [52,53]. This should modify the observed positron lifetime and CDB spectra. However, dislocations act as shallow positron traps and interact with positrons in a two-stage process. Once the positron is weakly localized at the dislocation core, it diffuses along the dislocation line and annihilates with deep traps, mainly vacancy-like defects anchored to the dislocation elastic field [54–56]. This dislocation-vacancy complex increases the positron lifetime by 15–34 ps respect the expected for isolated defects [57–59]. Also, grain boundaries and triple-grain points are defective regions that behave as vacancy-like complex traps. Furthermore, the studied materials have a high density of Y-O particles that are expected to exhibit a high positron affinity. CuYE and CuYME exhibit a fine-grained microstructure with a grain mean size ~500 nm, allowing a significant fraction of positron to reach the grain boundaries and annihilate with the vacancy-like defects, nanovoids or particles located there. The fraction of positrons that interact with grain boundaries is strongly dependent on the grain size and becomes significant when it is of the order of magnitude of the positron diffusion length, ~300 nm for defect-free Cu [60,61].

This submicrometric grained microstructure and defects produce at ECAP processing, causes the overall increase of the positron lifetime observed for CuYE and CuYME compared with the τ values of their unprocessed CuY and CuYM counterparts, which have a larger micrometric mean grain size. Before the recovery stage there is only a difference of ~10 ps in the τ values for ECAP materials because also as-HIP materials retain a high density of defects that hinder the effect of the grain boundaries, producing trapping saturation. As the recovery progresses and the minimum τ value is reached the difference increases to $\tau_{CuYE} - \tau_{CuY} \cong 40ps$ and $\tau_{CuYM} - \tau_{CuYME} \cong 25$ ps for each material, that also correlates with the initial larger grain size and lower τ values before ECAP processing. The difference in the number of ECAP processing steps should not have a significant impact in the measured positron lifetimes because even though the density of defects strongly depends on the number of ECAP passes, saturation is achieved after between the 4th-5th pass [62,63]. It is common to observe a decrease of the density of induced defects for a higher number of passes due to dynamic recovery process activated after achieving a certain degree of strain in the material, which has been also observed in Cu and other severe plastic deformed materials processed with techniques that allow accumulative processing such as HPT (High-Pressure Torsion) [64].

The behavior of τ correlates with the changes observed in the relative S-W plots, where there is a slight overall shift of the S parameter to higher values after ECAP processing, indicating that the fraction of positron annihilating with low-momentum electrons increases, and therefore points out to trapping and annihilation with open volume defects (see Figs. 7 and 8). Fig. 9 showed that for CuY the behavior of the S parameter as a function of temperature matched the positron lifetime behavior shown in Fig. 3(a). As S-W plots seem to indicate that all the alloys present the same kind of open-volume defects, it might be the case that the similarity between S parameter and positron lifetime that CuY presents, is also exhibited by the rest of the studied samples. Fig. 10 contains the evolution of S parameter as a function of the annealing temperature for the four studied samples. It is evident that for the non-processed samples (Fig. 10 (a)) the S parameter replicates the distribution over temperature that positron lifetime shown in Fig. 3(a). For ECAP processed alloys, the similarity is less clear but it is still present. CuYE sample, exhibits a minimum in the 600 – 700 °C region in both S parameter and positron lifetime distributions, followed by an increase; and CuYME shows the minimum slightly shifted to lower temperatures.

This correlates with the CDB curves that present a higher fraction of positrons annihilating with low-momentum electrons, i.e $p_L \leq 3 \times 10^{-3} m_0 c$ in the processed materials (Figs. 4 and 5). The CDB curves of CuY show the decrease of the CDB curve values at low momentum as the annealing temperature increases and progress the recovery of the Cu matrix with the annealing out of vacancies and vacancy clusters (see Fig. 6). This effect is hindered in the CDB as the

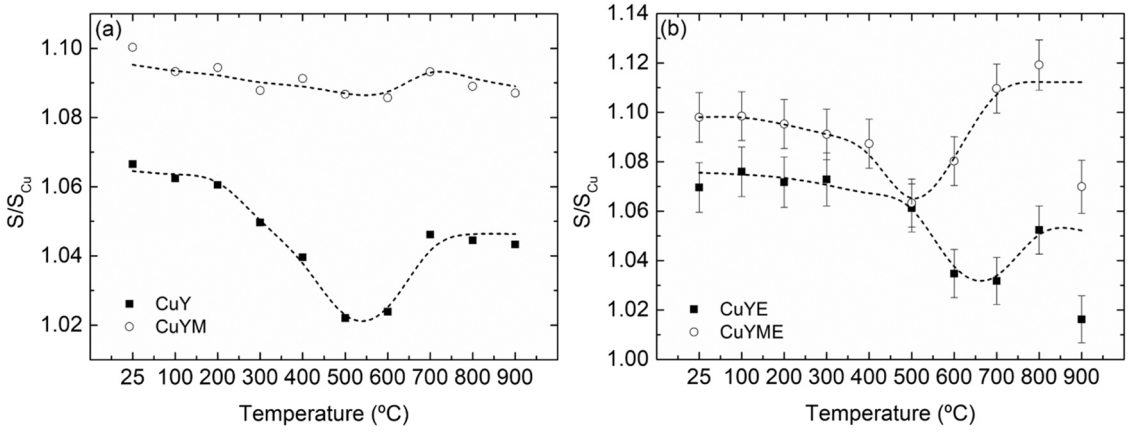

Fig. 10. S parameter as a function of the annealing temperature for (a) CuY and CuYM, and (b) CuYE and CuYME.

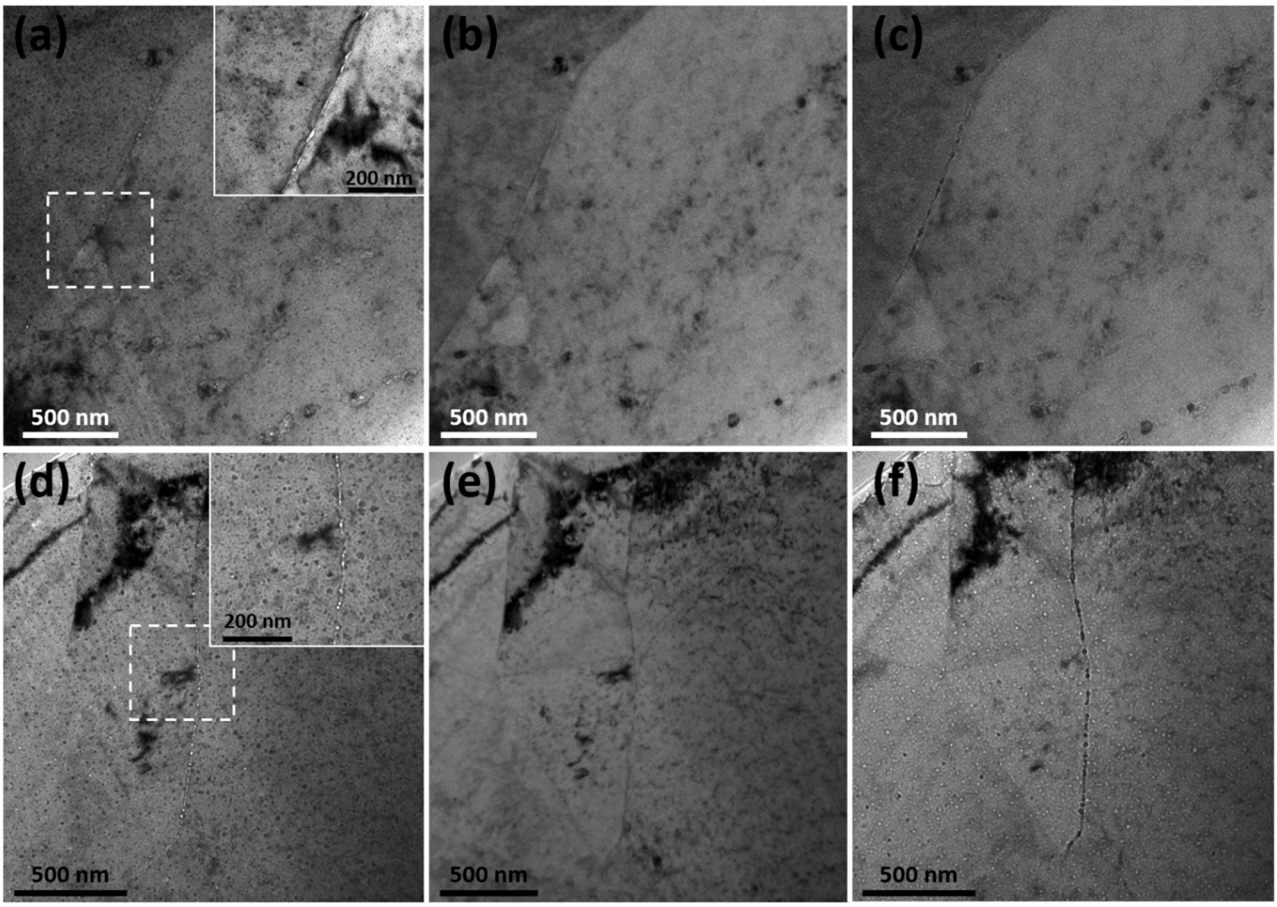

Fig. 11. TEM through-focal images of in CuY samples: after annealing at 600 °C ((a)-Under focused, (b)-Focused, (c)-Over focused) and after annealing at 900 °C (°C ((d)-Under focused, (e)-Focused, (f)-Over focused)). A detailed image is included for the white squared in images.

grain size of the materials decrease due to the signal coming from positrons annihilating at grain boundary defects, such as vacancy clusters, nanocavities or Y-O particles.

The CDB curves of all the studied reinforced Cu materials exhibits an overall similar structure in the high-momentum region, $p_L \geq 10 \times 10^{-3} m_0 c$ (see Figs. 4 and 5) to the observed in Fig. 6 for the Y_2O_3, and in particular to the Y_2O_3/Y ratio curve, disclosing the effect of the reinforcing Y-O oxides dispersion on the positron trapping characteristics [65,66]. Fig. 4 shows an increase in the high moment region of the CBD curves with increasing annealing temperature 300–600 °C for CuY, accompanied by the development of a structure similar to that observed for the Y_2O_3/Y ratio curve (see Fig. 6). The result indicates that positrons annihilate with oxygen core electrons and that there is an increase of the fraction of positrons trapped in defects whose chemical environment is rich in oxygen as recovery proceeds. CuYM, CuYE and CuYME exhibit a similar behavior, although this trend is partially masked by the signal coming from other positron traps (see Figs. 4 and 5). Numerous works have been published showing that positron annihilation spectroscopy is capable of characterizing the features associated to the presence of Y_2O_3 and Y oxides in ODS steels [67–70]. However, there is still a certain degree of controversy in the interpretation of some results because the positron can annihilate in the Y_2O_3 particles, or similar oxides, or in defects associated with these particles such as nanovoids or gas bubbles at the matrix/particle interface [67–70].

The characteristic positron lifetime for Y_2O_3 is not clearly established due to the extreme difficulty of obtaining good reference pure Y_2O_3 samples and the fact that this oxide has a high density of intrinsic structural lattice defects [65]. As previously appointed, measurements performed in our laboratory of sintered high purity nanopowder compacts of Y_2O_3 gave a positron lifetime value of (229 ± 2) ps, that agrees with the single result of (239 ± 6) ps that has been published in the literature to our knowledge [71]. These values are higher than the measured lifetime of our samples, indicating that there is no positron trapping saturation at the reinforcing Y-O particles. Moreover, Y-O particles are extremely stable and do not undergo significant changes in the temperature range of the isochronous treatment. Therefore, the results obtained for the reinforced Cu materials are consistent with the presence of stable vacancy-aggregates or nanocavities after the recovery stage associated with Y-O particles. These defects have to be at the interface of the Cu/Y-O particles or associated with impurities or particles at the grain boundaries since they are not stable at that temperature in the pure Cu matrix [46–49]. Also, this is consistent with results obtained from positron studies performed in reinforced steels with a dispersion of Y_2O_3 nanoparticles [67–69,72]. If the only surviving positron trapping sites after recovery were the Y-O particles there would only have been two possibilities that are not observed: i) saturation by positron trapping, in which case recovery would not have been observed, or ii) the positron lifetime spectra would have been resolved in two components: one corresponding to the bulk and the other to the reinforcing particles. The possibility that a fraction of annihilations occurs at the matrix of the Y-O and contribute to the mixed set of annihilation sites that gives a single unresolved positron lifetime cannot be excluded.

The most startling change observed in Fig. 3 is the increase of the lifetime τ after the recovery stage, to reach an almost constant value for temperatures 100 °C above that at which the minimum τ value

was reached. In this temperature range the microhardness does not experiment a significative change within the experimental uncertainty and grain growth occurs for CuYE and CuYME, increasing their mean grain size to (2.8 ± 1.5) μm and (2.1 ± 1.2) μm after the annealing treatment at 900 °C, respectively (see Fig. 1). Coarsening or dissolution of the Y-O particles was not observed. This high thermal stability of the particles is responsible for retaining at temperatures as high as 900 °C some of the microhardness enhancement achieved by ECAP processing.

This increase of τ correlates with the shift of the S parameter to higher values for all the materials (see Fig. 7(b)-(d) and 8 (a)-(b)) after finishing the recovery process, and that is clearly observed in Fig. 9 for CuY. As the annealing treatments progress up to temperatures of 700/800 °C, the CDB curves present their lower overall value in the intermediate momentum region, $p_L \approx 5 - 30(10^{-3} m_0 c)$, with the distinctive structure of peaks associated to the positron annihilation with core electrons of the oxygen anions revealed in reference CDB_{Y2O3}/CDB_Y normalized spectrum (see Fig. 4(b), (d) and Fig. 5(b), (d)). Such a behavior, together with the τ values observed of ~(160 ± 4) ps for ECAP unprocessed and ~(176 ± 3) ps and processed materials, respectively, is consistent with positron trapping and annihilation at vacancy-like defects and nanovoids associated to the Y-O particles. Furthermore, at these high temperatures, vacancy clusters will not survive in the pure Cu matrix, and they must be stabilized by the interaction with other defects or impurities, such as the interface of the Y-O particles or the presence of gas impurities inside the vacancy cluster of bubble as other works have reported in ODS steels [70,73,74]. Furthermore, Figs. 7 and 8 shows that the S-W pairs do not follow any consistent linear trend between 700 and 900 °C. The Fig. 9 for CuY shows particularly clear this behavior, with the S-W pairs cluster around a value within the experimental uncertainties. This is the expected behavior for positron trapping saturation at one type of dominant defect, showing that the concentration of these vacancy-type defects, like nanocavities due to the high value of the S parameter, remains high at that temperature regimen.

In order to understand the formation of these defects after the recovery stage, it is important to point out the role of the vacancy mobility and the formation of a high density of thermal vacancies at the temperatures above the recovery state. The equilibrium concentration of thermally generated vacancies in Cu grows exponentially at temperatures above ~620 °C [32]; however, in pure Cu they annealed out during cooling inside the furnace. At those high temperatures, vacancy diffusion is active, and they interact with the grain boundaries and the Y-O particle interfaces where they can be stabilized, forming vacancy complexes or promoting vacancy clustering and subsequent growth of nanovoids [70,73,74].

Direct TEM observations support these results. The presence of nanovoids was studied by bright-field TEM using a through-focal technique, being the under/over focus distance of 0.5 μm. The observations were carried out on CuY samples in the as-HIP state, and in CuY samples after the annealing treatment at 600 °C and 900 °C. Fig. 11 shows the presence of nanovoids at the grain boundaries and associated to some Y-O particles after annealing at 600 °C and 900 °C, being the density number of nanovoids higher for sample annealed at the higher temperature (see Fig. 10 (d)-(f)). These nanovoids exhibit contrast characteristics similar to those reported for Ar-decorated cavities in an ODS-9CrWVTaTi steel mechanically alloyed with 0.5 wt% of Y_2O_3 and Ti, reported previously [42]. In the sample annealed at 600 °C, the nanovoids are mainly located on grain boundaries and in the annealed sample at 900 °C they appear both randomly dispersed in the matrix associated with Y-O particles and on the grain boundaries. These nanocavities should be produced by vacancy aggregation of thermal generated vacancies at temperatures higher than the end of the recovery since their density is much lower for the material annealed at 600 °C (see Fig. 11 (a)-(c)).

At the recovery, temperatures below 600–700 °C, the dissolution of vacancy-clusters or vacancy-complexes defects in the Cu matrix and their migration of vacancies as the recovery progresses can generate their aggregation at the grain boundaries and at the Y-O/matrix interface, resulting in the formation of the observed nanocavities. Vacancy aggregates or nanovoids have large characteristic lifetimes that contribute to the value of the observed lifetime (see Table 1), but due to their low population at the end of the recovery, the overall contribution to the measured positron lifetime is small, especially for the CuY with the larger grain size and the less homogeneous dispersion of Y-O particles. As the recovery progresses, the decrease of the positron traps in the Cu matrix, such as interstitials or dislocations, increases the mean diffusion length of positrons with the decreasing population of defects and allows the positrons to increase their mean diffusion length, increasing the fraction of positrons that annihilate with more sparse defects associated to the grain boundaries or reinforcing Y-O particles, as the observed nanocavities by TEM (see Fig. 11) [75].

Several authors have previously reported the formation of vacancy aggregates or nanovoids, that are stable at high temperatures, in ODS steels produced by a pulvimetallurgical route that are reinforced with a dispersion of Y_2O_3 nanoparticles [70,76,77]. Their results using Positron Annihilation Spectroscopy and TEM confirm the hypothesis that the interface of the matrix and the Y_2O_3 act as effective sinks for vacancies and promotes the formation of nanovoids. There is a controversy whether the observed increase of the positron lifetime associated with these defects and their stability at a high temperature is associated with the presence of residual gas inside the nanovoids, that was introduced as an interstitial impurity at the milling phase of the production process. It is well known, form studies of pure Cu implanted with different gases species, H, He, Ar or Kr, that bubbles are formed after annealing treatments at elevated temperatures, which can be observed at temperatures higher than 820 °C (upper temperature of the experiments) [41,78–80]. The measured CuY and CuYM lifetimes after annealing at the highest temperatures have negligible difference of ± 4 ps, that is too short to be attributed to the presence of residual Ar inside the vacancy aggregates or nanovoids. The presence of residual gas in the CuY is unlikely because the powder has not been milled, while CuYM was milled in an Ar + 10%H atmosphere. Therefore the presence of residual gas inside the vacancy aggregates should be discarded since the expected lifetime for positrons in inert-gas bubbles should be $\tau = (\lambda_{surf} + \lambda_{gas})^{-1}$ [81] (λ_{surf} corresponds to the surface state annihilation rate of positrons at the surface of the metal and λ_{gas} with the atoms of the gas), which predicts a difference in the expected τ between empty nanocavities of vacancies aggregates and bubbles that were not observed between the positron lifetime results of CuY and CuYM (see Fig. 3).

5. Conclusions

To investigate the effects of the temperature in the microstructure and the evolution of the defects in Cu-0.8 wt%Y produced following two alternative powder metallurgical routes positron annihilation measurements have been performed after isochronal annealing treatments from room temperature to 900 °C in samples in the as HIP state and after ECAP processing. The work leads to these main results:

– Experiments revealed the presence of vacancy-like defects, vacancy aggregates and nanocavities, irrespective of the starting conditions of the samples. Annealing suggests a recovery process

(600–700 °C) due to an overall decrease in defect concentrations, some of them (corresponding to nanocavities) that are very stable at temperatures as high as 900 °C.
- Milling before HIP sintering produces a more refined and homogeneous microstructure prior to the ECAP processing. Lifetime measurements reveal that full recovery of the microstructure is not achieved, being the concentration of stable defects after the recovery stage higher for the CuYM, whose initial powder was milled, and for the ECAP processed materials.
- Annealing treatments at temperatures above 600–700 °C produce an unexpected increase of the measured positron lifetime and the S shape parameter, and a different trend for the S-W plots with the annealing temperature. The formation of these defects is attributed to the interaction of thermal activated vacancies with the Y-O particles, where the vacancies are trapped at the matrix/particle interfaces and form aggregates and nanocavities. This result has already been observed for ODS steels reinforced with a dispersion of nanometric Y_2O_3 particles [70,72–74]. CuYM lifetime after annealing above 700 °C is very similar to the observed for the CuY alloys, the same as CuYE and CuYME, indicating that the defects should correspond to nanocavities and not to bubbles filled with residual gas introduced in the copper matrix during the milling step of the production of CuYM, where an Ar + 10%H atmosphere is present.
- CDB results show that the vacancy aggregates are associated with the Y-O particles, growing at the matrix/particle interface, and they are responsible for the stability of the microstructure with the temperature. CuYE and CuYME alloys retain part of the microhardness that was achieved after ECAP processing after annealing at 900 °C.

CRediT authorship contribution statement

R. Domínguez-Reyes: Conceptualization, Methodology, Software, Validation, Formal Analysis, Investigation, Writing. **M.A. Monge:** Conceptualization, Methodology, Software, Investigation, Writing. **B. Galiana:** Methodology, Software, Investigation, Resources, Writing. **Y. Ortega:** Investigation, Writing. **A. Muñoz:** Conceptualization, Resources, Writing. **G. Carro-Sevillano:** Conceptualization, Resources.

Data Availability

The raw/processed data required to reproduce these findings cannot be shared at this time as the data also forms part of an ongoing study.

Declaration of Competing Interest

The authors declare that they have no known competing financial interests or personal relationships that could have appeared to influence the work reported in this paper.

Acknowledgements

This research was supported by the Spanish Ministerio de Economia y Competitividad (MINECO) in the form of Project ENE2015-70300-C3-2-R and by the Regional Government of Madrid (Spain) through TECHNOFUSIÓN(III)CM (S2018/EMT-4437), and Comunidad de Madrid (Spain) - multiannual agreement with UC3M ("Excelencia para el Profesorado Universitario" - EPUC3M14) - Fifth regional research plan 2016–2020; and also Spanish Ministerio de Ciencia e Innovación through project DAMAINSOL [grant number RTI2018-101020-B-I00].

References

[1] S.J. Zinkle, Applicability of copper Alloys for DEMO high heat flux components, Phys. Scr. 2016 (T167) (2016) 014004, https://doi.org/10.1088/0031-8949/2015/T167/014004
[2] J.H. You, Copper matrix composites as heat sink materials for water-cooled divertor target, Nucl. Mater. Energy 5 (2015) 7–18, https://doi.org/10.1016/j.nme.2015.10.001
[3] Y. Sumino, H. Watanabe, N. Yoshida, The microstructural evolution of precipitate strengthened copper alloys by varying temperature irradiation, J. Nucl. Mater. 386–388 (2009) 654–657, https://doi.org/10.1016/j.jnucmat.2008.12.249
[4] M. Hatakeyama, H. Watanabe, M. Akiba, N. Yoshida, Low void swelling in dispersion strengthened copper alloys under single-ion irradiation, J. Nucl. Mater. 307–311 (2002) 444–449, https://doi.org/10.1016/S0022-3115(02)01252-7
[5] J.R. Groza, J.C. Gibeling, Principles of particle selection for dispersion-strengthened copper, Mater. Sci. Eng. A 171 (1993) 115–125, https://doi.org/10.1016/0921-5093(93)90398-X
[6] D. Stork, P. Agostini, J.L. Boutard, D. Buckthorpe, E. Diegele, S.L. Dudarev, C. English, G. Federici, M.R. Gilbert, S. Gonzalez, A. Ibarra, C. Linsmeier, A.L. Puma, G. Marbach, L.W. Packer, B. Raj, M. Rieth, M.Q. Tran, D.J. Ward, S.J. Zinkle, Materials R&D for a timely DEMO: key findings and recommendations of the EU Roadmap Materials Assessment Group, Fusion Eng. Des. 89 (2014) 1586–1594, https://doi.org/10.1016/j.fusengdes.2013.11.007
[7] S.A. Fabritsiev, S.J. Zinkle, B.N. Singh, Evaluation of copper alloys for fusion reactor divertor and first wall components, J. Nucl. Mater. 233–237 (1996) 127–137, https://doi.org/10.1016/S0022-3115(96)00091-8
[8] M. Li, S.J. Zinkle, Physical and mechanical properties of copper and copper alloys, Compr. Nucl. Mater. 4 (2012) 667–690, https://doi.org/10.1016/B978-0-08-056033-5.00122-1
[9] G. Li, B.G. Thomas, J.F. Stubbins, Modeling creep and fatigue of copper alloys, Metall. Mater. Trans. 31A (2000) 2491–2502, https://doi.org/10.1007/s11661-000-0194-z
[10] D. Stork, P. Agostini, J.L. Boutard, D. Buckthorpe, E. Diegele, S.L. Dudarev, C. English, G. Federici, M.R. Gilbert, S. Gonzalez, A. Ibarra, C. Linsmeier, A. Li Puma, G. Marbach, P.F. Morris, L.W. Packer, B. Raj, M. Rieth, M.Q. Tran, D.J. Ward, S.J. Zinkle, Developing structural, high-flux and plasma facing materials for a near-term DEMO fusion power plant: The EU assessment, J. Nucl. Mater. 455 (2014) 277–291, https://doi.org/10.1016/j.jnucmat.2014.06.014
[11] H.R. Brager, Effects of neutron irradiation to 63 dpa on the properties of various commercial copper alloys, J. Nucl. Mater. 141–143 (1986) 79–86, https://doi.org/10.1016/S0022-3115(86)80014-9
[12] B.N. Singh, A. Horsewell, D.S. Gelles, F.A. Garner, Void swelling in copper and copper alloys irradiated with fission neutrons, J. Nucl. Mater. 191- 194 (1992) 1172–1176, https://doi.org/10.1016/0022-3115(92)90659-9
[13] Y. Shimomura, I. Mukouda, K. Sugio, The influence of dynamical structural relaxation of point defect clusters on void formation in irradiated copper, J. Nucl. Mater. 25 (1) (1997) 61–71, https://doi.org/10.1016/S0022-3115(97)00243-2
[14] B.N. Singh, D.J. Edwards, M. Eldrup, P. Toft, Effects of heat treatments and neutron irradiation on microstructures and physical and mechanical properties of copper alloys, J. Nucl. Mater. 249 (1997) 1–16, https://doi.org/10.1016/S0022-3115(97)00184-0
[15] G. Carro, A. Muñoz, M.A. Monge, B. Savoini, R. Pareja, Microstructural and mechanical characterization of Cu-0.8 wt%Y, Fusion Eng. Des. 98–99 (2015) 1941–1944, https://doi.org/10.1016/j.fusengdes.2015.06.113
[16] G. Carro, A. Muñoz, M.A. Monge, B. Savoini, A. Galatanu, M. Galatanu, R. Pareja, Thermal conductivity and diffusivity of Cu-Y alloys produced by different powder metallurgy routes, Fusion Eng. Des. 124 (2017) 1156–1160, https://doi.org/10.1016/j.fusengdes.2017.01.017
[17] G. Carro, A. Muñoz, M.A. Monge, B. Savoini, Fabrication and characterization of dispersion strengthened Cu-0.8%Y, Fusion Eng. Des. 154 (2020) 111548, https://doi.org/10.1016/j.fusengdes.2020.111548
[18] B.N. Singh, A. Horsewell, P. Toft, D.J. Edwards, Temperature and dose dependencies of microstructure and hardness of neutron irradiated OFHC copper, J. Nucl. Mater. 224 (1995) 131–140, https://doi.org/10.1016/0022-3115(95)00054-2
[19] M. Victoria, N. Baluc, C. Bailat, Y. Dai, M.I. Luppo, R. Schaublin, B.N. Singh, The microstructure and associated tensile properties of irradiated fcc and bcc metals, J. Nucl. Mater. 276 (2000) 114–122, https://doi.org/10.1016/S0022-3115(99)00203-2 https://doi.org/10.1016/S0022-3115(99)00203-2.
[20] P. Kirkegaard, N.J. Pedersen, M.M. Eldrup. (1989). PATFIT-88: A Data-Processing System for Positron Annihilation Spectra on Mainframe and Personal Computers. Risø National Laboratory, Denmark (1989). Risø-M No. 2740.
[21] M. Furukawa, Y. Iwahashi, Z. Horita, The shearing characteristics associated with equal-channel angular pressing, Mater. Sci. Eng. A 257 (2) (1998) 328–332, https://doi.org/10.1016/S0921-5093(98)00750-3
[22] S. Tao, L. Yulong, D. Qiong, L. Yuanyong, Optimal pressing route for continued equal channel angular pressing by finite element analysis, Mater. Sci. Eng. A 466 (1–2) (2007) 166–171, https://doi.org/10.1016/j.msea.2007.02.068
[23] M.J. Puska, P. Lanki, R.M. Nieminen, Positron affinities for elemental metals, J. Phys.: Condens. Matter 1 (25) (1989) 6081–6094, https://doi.org/10.1088/0953-8984/1/35/008
[24] M.J. Puska, M. Šob, G. Brauer, T. Korhonen, First-principles calculation of positron lifetimes and affinities in perfect and imperfect transition-metal carbides and nitrides, Phys. Rev. B 49 (1994) 10947–10957, https://doi.org/10.1103/PhysRevB.49.10947

[25] Y. Ortega, M.A. Monge, R. Pareja, The precipitation process in Mg–Ca–(Zn) alloys investigated by positron annihilation spectroscopy, J. Alloy Compd. 463 (1–2) (2008) 62–66, https://doi.org/10.1016/j.jallcom.2007.09.044

[26] C.-Y. Xi, B.-J. Ye, H.-M. Weng, X.-Y. Zhou, R.-D. Han, Coincidence Doppler Broadening Study of Elemental Metals, Chin, J. Chem. Phys. 19 (2006) 203, https://doi.org/10.1360/cjcp2006.19(3).203.4

[27] M. Maekawa, A. Kawasuso, Z.Q. Chen, M. Yoshikawa, R. Suzukic, T. Ohdaira, Structural defects in SiO2/SiC interface probed by a slow positron beam, Appl. Surf. Sci. 244, 1-4 244 (2005) 322–325, https://doi.org/10.1016/j.apsusc.2004.10.085

[28] A.C. Kruseman, A. van Veen, H. Schut, P.E. Mijnarends, Buried oxide and defects in oxygen implanted Si monitored by positron annihilation, J. Appl. Phys. 90 (2001) 1179–1187, https://doi.org/10.1063/1.1380411

[29] J.-D. Liu, J. Zhang, L.-J. Zhang, Y.-P. Hao, W.-F. Guo, B. Cheng, B.-J. Ye, Theoretical study on the positron annihilation in Rocksalt structured magnesium oxide, Chin. Phys. B 20 (2011) 057802, https://doi.org/10.1088/1674-1056/20/5/057802

[30] L. Liszkay, C. Corbel, L. Baroux, P. Hautojarvi, M. Bayhan, A.W. Brinkman, S. Tatarenko, Positron trapping at a small vacancy cluster in thin polycrystalline CdTe films deposited on glass, Appl. Phys. Lett. 64 (1994) 1380–1382, https://doi.org/10.1063/1.111994

[31] B. Somieski, T.E.M. Staab, R. Krause-Rehberg, The data treatment influence on the spectra decomposition in positron lifetime spectroscopy Part 1: On the interpretation of multi-component analysis studied by Monte Carlo simulated model spectra, Nucl. Instrum. Methods A 381 (1) (1996) 128–140, https://doi.org/10.1016/0168-9002(96)00584-0

[32] T. Hehenkamp, T. Kurschat, W. Luhr-Tanck, Positron lifetime spectroscopy in copper, J. Phys. F. Met. Phys. 16 (8) (1986) 981–987, https://doi.org/10.1088/0305-4608/16/8/012

[33] R. Brusa, G.K.W. Deng, A. Zecca, Doppler-broadening measurements of positron annihilation with high-momentum electrons in pure elements, Nucl. Instrum. Methods B 194 (2002) 519–531, https://doi.org/10.1016/S0168-583X(02)00953-9

[34] K. Zhou, T. Zhang, Z. Wang, Positron lifetime calculation for possible defects in nanocrystalline copper, Phys. Scr. 90 (10) (2015) 105701, https://doi.org/10.1088/0031-8949/90/10/105701

[35] H.E. Schaefer, Investigation of thermal equilibrium vacancies in metals by positron annihilation, Phys. Status Solidi A 102 (1) (1987) 47–65, https://doi.org/10.1002/pssa.2211020104

[36] J. Čížek, I. Procházka, M. Cieslar, R. Kužel, J. Kuriplach, F. Chmelík, I. Stulíková, F. Bečvář, O. Melikhova, R.K. Islamgaliev, Thermal stability of ultrafine grained copper, Phys. Rev. B 65 (9) (2002) 094106⟨https://link.aps.org/doi/10.1103/PhysRevB.65.094106⟩.

[37] J.M.C. Robles, E. Ogando, F. Plazaola, Positron lifetime calculation for the elements of the periodic table, J. Phys. -Condens. Matter 19 (17) (2007) 176222, https://doi.org/10.1088/0953-8984/19/17/176222

[38] M. Eldrup, J.H. Evans, O.E. Mogensen, B.N. Singh, A positron annihilation investigation of defects in neutron irradiated copper, Rad. Eff. 54 (1981) 65–80, https://doi.org/10.1080/00337578108207128

[39] M. Eldrup, B.N. Singh, Studies of defects and defect agglomerates by positron annihilation spectroscopy, J. Nucl. Mater. 251 (1997) 132–138, https://doi.org/10.1016/S0022-3115(97)00221-3

[40] T.E.M. Staab, R. Krause-Rehberg, B. Kieback, Review positron annihilation in fine-grained materials and fine powders—an application to the sintering of metal powders, J. Mater. Sci. 34 (1999) 3833–3851, https://doi.org/10.1023/A:1004666003732

[41] M. Eldrup, B.N. Singh, Studies of defects and defect agglomerates by positron annihilation spectroscopy, J. Nucl. Mater. 251 (1997) 132–138, https://doi.org/10.1016/S0022-3115(97)00221-3

[42] S. Mantl, W. Triftshäuser, Defect annealing studies on metals by positron annihilation and electrical resistivity measurements, Phys. Rev. B 17 (1978) 1645–1652, https://doi.org/10.1103/PhysRevB.17.1645

[43] M. Eldrup, B.N. Singh, Study of defects annealing behavior in neutron irradiated Cu and Fe using positron annihilation and electrical conductivity, J. Nucl. Mater. 276 (2000) 269–277, https://doi.org/10.1016/S0022-3115(99)00186-5

[44] H. Ohkubo, Z. Tang, Y. Nagai, M. Hasegawa, T. Tawara, M. Kiritani, Positron annihilation study of vacancy-type defects in high-speed deformed Ni, Cu and Fe, Mater. Sci. Eng. A 350 (2003) 95–101, https://doi.org/10.1016/S0921-5093(02)00705-0

[45] M. Eldrup, B.N. Singh, D.J. Edwards, Y. Nagai, H. Ohkubo, M. Hasegawa, Neutron irradiated copper: Is the main positron lifetime component due to stacking fault tetrahedra? Mater. Sci. Forum 445–446 (2004) 21–25, https://doi.org/10.4028/www.scientific.net/MSF.445-446.21

[46] Y. Cheng, Z.-H. Jin, Y.W. Zhanga, H. Gao, On intrinsic brittleness and ductility of intergranular fracture along symmetrical tilt grain boundaries in copper, Acta Mater. 58 (7) (2010) 2293–2299, https://doi.org/10.1016/j.actamat.2009.11.033

[47] V. Slugen, J. Kuriplach, P. Ballo, P. Domonkos, G. Kögel, P. Sperr, W. Egger, W. Triftshäuser, V.M. Domankova, P. Kovac, I. Vavra, S. Stancek, M. Petriska, A. Zeman, Positron annihilation investigations of defects in copper alloys selected for nuclear fusion technology, Fusion Eng. Des. 70 (2) (2004) 141–153, https://doi.org/10.1016/j.fusengdes.2003.10.002

[48] R.R. Bourassa, B. Lengeler, The formation and migration energies of vacancies in quenched copper, J. Phys. F: Met. Phys. 6 (1976) 1405–1413, https://doi.org/10.1088/0305-4608/6/8/003

[49] I.K. Bishay, E. Hassan Aly, F.A. Saadallah, A study of annealing stages in commercial pure Cu using mechanical measurements and positron annihilation lifetime technique, Mater. Sci. Eng. A 527 (16–17) (2010) 3893–3897, https://doi.org/10.1016/j.msea.2010.02.074

[50] M. Li, P. Hu, Y. Zhang, Y. Chang, Enhancing performance of the CuCrZrTiV alloys through increasing recrystallization resistance and two-step thermomechanical treatments, J. Nucl. Mater. 543 (2021) 152482, https://doi.org/10.1016/j.jnucmat.2020.152482

[51] G. Carro, A. Muñoz, M.A. Monge, B. Savoini, A. Galatanu, M. Galatanu, R. Pareja, Thermal conductivity and diffusivity of Cu-Y alloys produced by different powder metallurgy routes, Fusion Eng. Des. 124 (2017) 1156–1160, https://doi.org/10.1016/j.fusengdes.2017.01.017

[52] T. Suo, Y.-L. Li, K. Xie, F. Zhao, K.-S. Zhang, Y.-Y. Liu, The effect of temperature on mechanical behavior of ultrafine-grained copper by equal channel angular pressing, Mater. Sci. Eng. A 527 (21–22) (2010) 5766–5772, https://doi.org/10.1016/j.msea.2010.05.046

[53] A. Hernández-Pérez, M. Eddahbi, M.A. Monge, A. Muñoz, B. Savoini, Microstructure and mechanical properties of an ITER-grade Cu–Cr–Zr alloy processed by equal channel angular pressing, Fusion Eng. Des. 98–99 (2015) 1978–1981, https://doi.org/10.1016/j.fusengdes.2015.06.180

[54] L.C. Smedskjaer, M. Manninen, M.J. Fluss, An alternative interpretation of positron annihilation in dislocations, J. Phys. F Met. Phys. 10 (1980) 2237–2249, https://doi.org/10.1088/0305-4608/10/10/019

[55] K. Hinode, S. Tanigawa, M. Doyama, Positron lifetimes in deformed copper, J. Phys. Soc. Jpn. 41 (1976) 2037–2042, https://doi.org/10.1143/JPSJ.41.2037

[56] Y. Kamimura, T. Tsutsumi, E. Kuramoto, Calculations of positron lifetimes in a jog and vacancies on an edge-dislocation line in Fe, Phys. Rev. B Condens Matter 52 (2) (1995) 879–885, https://doi.org/10.1103/PhysRevB.52.879

[57] S. Kupca, D.P. Kerr, B.G. Hogg, Z.S. Basinski, Positron annihilation in fatigued copper, Can. J. Phys. 52 (9) (1982) 140–144, https://doi.org/10.1139/p82-025

[58] I. Prochazca, J. Cizek, O. Melikhova, Z. Barnovska, Ultra-fine grained Copper prepared by high-pressure torsion: A positron annihilation study of microstructure evolution and lateral distribution of defects, 3rd International Conference of Nanotechnology, (2011) 231–237.

[59] K. Ito, H. Nakanishi, Y. Ujihira, Extension of the equation for the annihilation lifetime of ortho-positronium at a cavity larger than 1 nm in radius, J. Phys. Chem. B 103 (21) (1999) 4555–4558, https://doi.org/10.1021/jp9831841

[60] C. Hübner, T. Staab, R. Krause-Rehberg, On the interpretation of positron-annihilation data in powders and fine-grained materials, Appl. Phys. A 61 (2) (1995) 203–206, https://doi.org/10.1007/BF01538390

[61] R.M. Nieminen, in edited by W. Brandt and A. Dupasquier, Proceedings of the International School of Physics "Enrico Fermi"— Positron Solid State Physics (North Holland, Amsterdam, 1983) pp. 359–407.

[62] N. Lugo, N. Llorca, J.J. Suñol, J.M. Cabrera, Thermal stability of ultrafine grains size of pure copper obtained by equal-channel angular pressing, J. Mater. Sci. 45 (2010) 2264–2273, https://doi.org/10.1007/s10853-009-4139-7

[63] T. Kvačkaj, A. Kováčová, R. Kočiško, J. Dutkiewicz, L. Litynska-Dobrzy nska, J. Kansy, Relation between microstructural features and mechanical properties in oxygen free high conductivity copper after equal-channel angular pressing, Metal. Mater. 52 (6) (2014) 337–344, https://doi.org/10.4149/km_2014_6_337

[64] J. Čížek, M. Janeček, O. Srba, R. Kužel, Z. Barnovská, I. Procházka, S. Dobatkin, Evolution of defects in copper deformed by high-pressure torsion, Acta Mater. 59 (6) (2011) 2322–2329, https://doi.org/10.1016/j.actamat.2010.12.028

[65] M. Hartmanová, E. Morháčová, I. Travěnec, A.A. Urosovskaya, G.G. Knab, I.I. Korobkov, Defect structure and physical properties of Y2O3, Solid State Ion. 36 (3–4) (1989) 137–142, https://doi.org/10.1016/0167-2738(89)90157-4

[66] N.M. Tallan, R.W. Vest, Electrical properties and defect structure of Y2O3, J. Am. Ceram. Soc. 49 (8) (1966) 401–404, https://doi.org/10.1111/j.1151-2916.1966.tb15404.x

[67] V. Krsjak, Z. Szaraz, P. Hähner, Positron annihilation lifetime study of oxide dispersion strengthened steels, J. Nucl. Mater. 428 (1–3) (2012) 160–164, https://doi.org/10.1016/j.jnucmat.2011.11.058

[68] Y. Ortega, M.A. Monge, V. de Castro, A. Muñoz, T. Leguey, R. Pareja, Void formation in ODS EUROFER produced by hot isostatic pressing, J. Nucl. Mater. 386–388 (2009) 462–465, https://doi.org/10.1016/j.jnucmat.2008.12.145

[69] M. Šćepanović, V. de Castro, I. García-Cortés, F.J. Sánchez, T. Gigl, C. Hugenschmidt, T. Leguey, Characterization of open volume defects in Fe–Cr and ODS Fe–Cr alloys after He+ and Fe+ ion irradiations, J. Nucl. Mater. 538 (2020) 152230, https://doi.org/10.1016/j.jnucmat.2020.152230

[70] Y. Ortega, V. de Castro, M.A. Monge, A. Muñoz, T. Leguey, R. Pareja, Positron annihilation characteristics of ODS and non-ODS EUROFER isochronally annealed, J. Nucl. Mater. 376 (2) (2008) 222–228, https://doi.org/10.1016/j.jnucmat.2008.03.005

[71] L.C. Damonte, M.A. Taylor, J. Desimoni, J. Runco, PALS study on the defect structure of yttria-stabilized zirconia, Radiat. Phys. Chem. 76 (2) (2007) 248–251, https://doi.org/10.1016/j.radphyschem.2006.03.046

[72] R. Domínguez-Reyes, M.A. Auger, M.A. Monge, R. Pareja, Positron annihilation study of the vacancy clusters in ODS Fe–14Cr alloys, Philos. Mag. 97 (2017) 11–850, https://doi.org/10.1080/14786435.2017.1280621

[73] J. Alinger, G.R. Odette, S.C. Glade, B.D. Wirth, Y. Nagai, M. Hasegawa, ORNL Report, 2004.

[74] R. Rajaraman, G. Amarendra, C.S. Sundar, Defect evolution in steels: Insights from positron studies 6, 11, Special Issue: 15th International Conference on Positron Annihilation (ICPA-15) (2009) 2285–2290. https://doi.org/10.1002/pssc.200982112.

[75] T.E.M. Staab, R. Krause-Rehberg, B. Kieback, Review Positron annihilation in fine-grained materials and fine powders—an application to the sintering of metal powders, J. Mater. Sci. 34 (1999) 3833–3851, https://doi.org/10.1023/A:1004666003732

[76] V.S.M. Pereira, H. Schut, J. Sietsma, A study of the microstructural stability and defect evolution in an ODS eurofer steel by means of electron microscopy and positron annihilation spectroscopy, J. Nucl. Mater. 540 (2020) 152398, https://doi.org/10.1016/j.jnucmat.2020.152398

[77] V. Krsjak, T. Shen, J. Degmova, S. Sojak, E. Korpas, P. Noga, W. Egger, B. Li, V. Slugen, F.A. Garner, On the helium bubble swelling in nano-oxide dispersion-strengthened steels, J. Mater. Sci. Technol. 105 (2022) 172–181, https://doi.org/10.1016/j.jmst.2021.08.004

[78] Fundamental Aspects of Inert Gases in Solids, Sefles B: Physics, in: S.E. Donnelly, J.H. Evans (Eds.), 209 (Springer Science+ Business Media, LLC), 1990, , https://doi.org/10.1007/978-1-4899-3680-6

[79] A. Yabuuchi, T. Kihara, D. Kubo, M. Mizuno, H. Araki, T. Onishi, Y. Shirai, Effect of hydrogen on vacancy formation in sputtered Cu films studied by positron annihilation spectroscopy, Jpn. J. Appl. Phys. 52 (2013) 4R, https://doi.org/10.7567/JJAP.52.046501

[80] O. Kurnosikov, D.V. Kulikov, V.S. Kharlamov, H.J.M. Swagten, Yu.V. Trushin, Temperature-induced evolution of subsurface nanocavities in argon-implanted copper, Phys. Rev. B 84 (2011) 054109, https://doi.org/10.1103/PhysRevB.84.054109

[81] K.O. Jensen, R.M. Nieminem, Noble-gas bubbles in metals: molecular-dynamics simulations and positron states, Phys. Rev. B 36 (1987) 8219–8232, https://doi.org/10.1103/PhysRevB.36.8219